Eur. Phys. J. A **25**, 267–273 (2005)
DOI 10.1140/epja/i2005-10112-5

THE EUROPEAN PHYSICAL JOURNAL A

Theoretical description of the p d → p d η reaction near threshold

U. Tengblad[1,a], G. Fäldt[1,b], and C. Wilkin[2,c]

[1] Department of Radiation Sciences, Box 535, S-751 21 Uppsala, Sweden
[2] Department of Physics & Astronomy, UCL, London WC1E 6BT, UK

Received: 13 June 2005 / Revised version: 29 June 2005 /
Published online: 30 August 2005 –
Communicated by V. Vento

Abstract. The contributions of three different types of driving terms are included in the estimation of the $p\,d \to p\,d\,\eta$ reaction at low energies. Near threshold, it is predicted that a two-step model involving an intermediate pion should be the most important but, as the energy approaches the threshold for η production in the free nucleon-nucleon reaction, a pick-up mechanism with a spectator proton should become dominant. The total cross-sections are underestimated by about a factor of two compared with experimental data but the discrepancies in the angular distributions are more serious, with no sign in the data for the peaks corresponding to the pick-up diagram.

PACS. 25.10.+s Nuclear reactions involving few-nucleon systems – 13.60.Le Meson production – 14.40.Aq π, K, and η mesons

1 Introduction

The great interest in the production of heavy mesons near threshold started with measurements of the $p\,d \to {}^3\mathrm{He}\,\eta$ reaction, which showed a surprisingly strong cross-section with an anomalous energy dependence [1]. An impulse approximation description of the process, where the production takes place in nucleon-nucleon scattering, with the other nucleon in the deuteron being essentially a spectator, greatly underestimates the observed rate because of the high-momentum components required in the nuclear wave functions [2]. To share the large momentum transfer between the nucleons, a mechanism was proposed whereby a pion was produced in an initial $pp \to d\pi^+$ reaction to be followed by the production of the observed meson through a secondary $\pi^+ n \to \eta p$ process [3]. Near threshold, the kinematics are favourable for the final proton and deuteron to *stick* to form the observed ^{3}He. A quantum-mechanical evaluation of this suggestion [4] led to a cross-section that was only about a factor of two lower than a precise measurement of the reaction rate [5]. To understand the situation further, it would be helpful to look at other related final states.

The total cross-section for the $p\,d \to p\,d\,\eta$ reaction, where a final ^{3}He is not formed, was measured at two energies very close to threshold at Saclay [6]. A preliminary evaluation of the two-step model with an intermediate pion, that was successful in the description of the ${}^3\mathrm{He}\,\eta$ final state, gave very promising results when compared to these data [7]. Differential as well as total cross-sections for this reaction at higher energies have recently become available from Uppsala [8], to complement those obtained by the same group for the $p\,d \to {}^3\mathrm{He}\,\eta$ reaction [9]. The time therefore seems opportune to make a further theoretical investigation of the $p\,d\,\eta$ final state.

The kinematics of the Saclay experiment [6] are very close to those where a ^{3}He emerges and so it is not surprising that in this region the two-step model describes the process well, as it did for the ${}^3\mathrm{He}\,\eta$ final state [4]. On the other hand, as one approaches the threshold for η production in free nucleon-nucleon collisions, one expects a pick-up diagram, corresponding to a quasi-free $pn \to d\,\eta$ production on the neutron in the target, to dominate. Between these two extremes there is also the possibility of a contribution from the impulse approximation diagram with a quasi-free $pN \to pN\,\eta$ on a proton or neutron that is bound both initially and finally in the deuteron. Away from threshold, these terms may not be universally suppressed, as they are for ${}^3\mathrm{He}\,\eta$, because of the greater flexibility in the $p\,d\,\eta$ kinematics; in certain parts of phase space, the momentum transfers between initial and final deuterons are minimised.

The three types of contributions are described further in sect. 2, where the general kinematics are discussed. The following three sections are devoted to the evaluation of the cross-section distributions for the individual

[a] e-mail: ulla.tengblad@tsl.uu.se
[b] e-mail: goran.faldt@tsl.uu.se
[c] e-mail: cw@hep.ucl.ac.uk

terms. Uncertainties in the phases of the amplitudes lead us to neglecting interferences. This may not be too dangerous because the various models tend to populate different parts of what is a three-body phase space. More worrying is that we neglect also all final-state interactions *fsi*. Now, unlike the $\eta\,^3$He case [5], there is no simple prescription for the inclusion of such effects when there is an *fsi* between more than one pair of particles. Experimentally a threshold enhancement is seen only in the $\eta\,d$ invariant-mass distribution, whereas that for $p\,d$ looks like phase space, despite the presence of the strong interaction which could lead to the formation of the ^{3}He [8]. The results for the total cross-sections, and both angular and invariant-mass distributions, are compared with experiment in sect. 6. The overall production rate is underestimated by about a factor of two, which is rather similar to that found for the $p\,d \to {}^3\mathrm{He}\,\eta$ reaction within a similar theoretical approach. However, the angular distributions of both the proton and deuteron show discrepancies with respect to the data, with the latter showing no signs of the forward deuteron and backward proton peaks corresponding to the spectator proton of the pick-up mechanism. Our conclusions are drawn in sect. 7.

2 Defining the problem

The three classes of diagrams that we evaluate for the $p\,d \to p\,d\,\eta$ reaction are illustrated in fig. 1. It is generally assumed that the neutron-exchange diagram (a) dominates the reaction above the free NN threshold and, indeed, it is this hypothesis that is the basis of the extraction of the quasi-free $pn \to d\,\eta$ cross-section on a moving neutron from $p\,d \to p\,d\,\eta$ data [10]. Below threshold, the presence of a spectator proton in this case will bias the distributions to low $d\,\eta$ invariant masses.

The impulse approximation diagram of fig. 1b is often used to model coherent reactions on the deuteron at high energies, where the momentum transfer to the final deuteron can be small. There is, of course, a second term where the η production takes place on the neutron and some theoretical model is required to deduce the relative phases of the spin-isospin input amplitudes needed to make reliable estimates here [11]. A final-state interaction between the proton and deuteron to form an ^{3}He for either the diagrams in fig. 1a, b would lead to the triangle graph, whose contribution has been shown to be small for $p\,d \to {}^3\mathrm{He}\,\eta$ [2]. That they are not necessarily negligible here is due to the fact that the final dp pair does not have to emerge with low excitation energy.

The centre-of-mass differential cross-section for the $p\,d \to p\,d\,\eta$ reaction is determined by the matrix element $\mathcal{M}$ through

$$\mathrm{d}\sigma = \frac{1}{4p\sqrt{s}} \left\{ \frac{1}{6} \sum_{\text{spins}} |\mathcal{M}|^2 \right\} (2\pi)^4 \delta^4(P_i - P_f) \prod_{j=1}^{3} \frac{\mathrm{d}^3 p_j}{(2\pi)^3 2E_j}\,, \tag{2.1}$$

where the sum is over the spin projections in the initial and final states. Here $P_i^2 = P_f^2 = s$ is the square of the total c.m. energy, $(E_j, \boldsymbol{p}_j)$ are the energy and three-momentum of the reaction products, and $\boldsymbol{p}$ is the initial proton c.m. momentum.

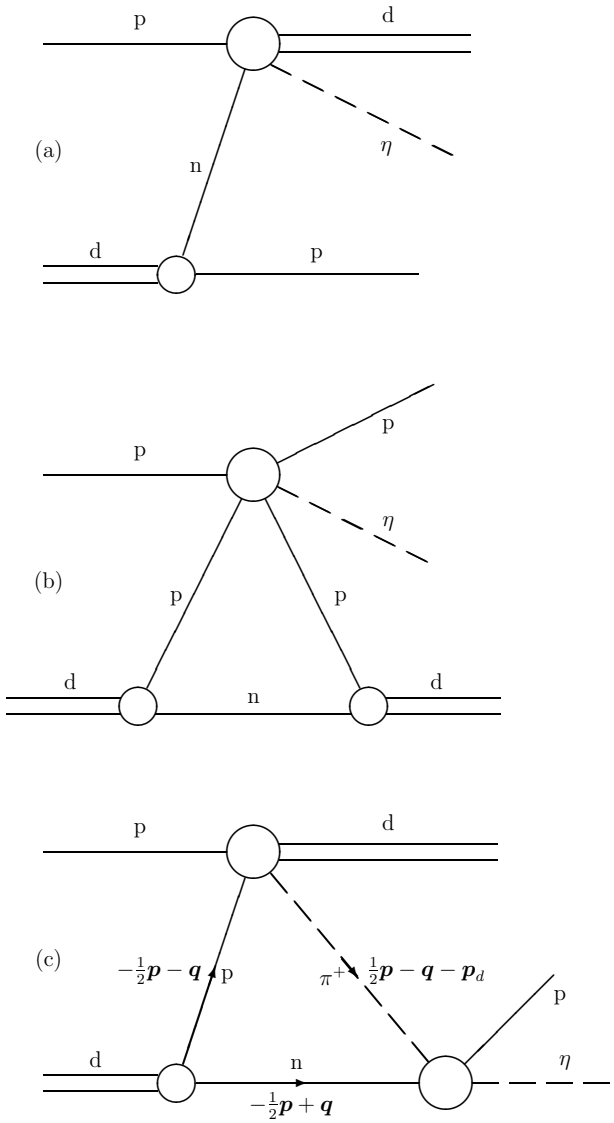

Fig. 1. Three classes of diagrams relevant for the $p\,d \to p\,d\,\eta$ reaction. (a) The pick-up term which dominates above the NN threshold. (b) The impulse (triangle) diagram. There is a similar contribution with the internal proton and neutron interchanged. (c) The two-step model with an intermediate pion. The contribution where the π^+ is replaced by a π^0 is related to this through isospin invariance.

Experimental distributions have been given in terms of the angles of the final particles and the invariant masses of pairs of such particles [8]. For this purpose it is convenient to reduce the phase-space factors to:

$$\mathrm{d}\sigma = \frac{1}{4p\,s} \left\{ \frac{1}{6} \sum_{\text{spins}} |\mathcal{M}|^2 \right\} \frac{1}{256\pi^5}\, p_d\, \mathrm{d}\Omega_d\, p_\eta^*\, \mathrm{d}\Omega_\eta^*\, \mathrm{d}m_{\eta p}\,, \tag{2.2}$$

where the final-deuteron energy and momentum $(E_d, \boldsymbol{p}_d)$, as well as the angles Ω_d, are evaluated in the overall c.m. system while those of the η are evaluated in the ηp rest frame, where the invariant mass is given by

$$m_{\eta p}^2 = s + m_d^2 - 2\sqrt{s}\,E_d\,. \tag{2.3}$$

Analogous formulae follow immediately for the other two combinations of variables.

3 The pick-up contribution

Though there is an enhancement at threshold, the energy dependence of the $pn \to d\,\eta$ total cross-section is broadly consistent with s-wave production up to an excess energy of at least 60 MeV [10]. At threshold there is only one c.m. amplitude, which can be written as

$$\mathcal{M}(pn \to d\eta) = u_{n_c}^\dagger \left[G\sqrt{s_{pn}}\,\boldsymbol{p}_n \cdot \boldsymbol{\epsilon}_d\right] u_p\ , \tag{3.1}$$

where $\boldsymbol{p}_n$ is the initial momentum and the c.m. energy $\sqrt{s_{pn}}$ arises from the reduction from a relativistic form. Here u_p and u_{n_c} are proton and charge-conjugate neutron Pauli spinors, respectively.

In terms of the amplitude G, the total $pn \to d\,\eta$ cross-section is

$$\sigma_T(pn \to d\eta) = \frac{1}{8\pi} p_\eta^* p_p^*\,|G|^2\,, \tag{3.2}$$

where the p^* are evaluated in the pn c.m. frame where the total energy equals $m_{\eta d}$. The experimental data are then consistent with a value of $|G|^2 = (0.046 \pm 0.011)$ fm^4 [10].

The spin-averaged amplitude squared for the pick-up term of fig. 1a reduces to

$$\frac{1}{6}|\mathcal{M}(pd \to pd\eta)|^2 = \frac{1}{8\pi}[(2\pi)^3 2m_d](2m_{\eta d}p_p^*)^2\,|G|^2\,\left\{\tilde{\varphi}_S(q)^2 + \tilde{\varphi}_D(q)^2\right\}. \tag{3.3}$$

Here the deuteron wave functions $\tilde{\varphi}_S(q)$ and $\tilde{\varphi}_D(q)$ are normalised by

$$\int_0^\infty q^2\,\left\{\tilde{\varphi}_S(q)^2 + \tilde{\varphi}_D(q)^2\right\}\,\mathrm{d}q = 1\,. \tag{3.4}$$

They are evaluated at a momentum-squared of

$$\boldsymbol{q}^2 = \frac{m_d^2}{E_{di}^2}(-\tfrac{1}{2}p - p_{p\|})^2 + \boldsymbol{p}_{p\perp}^2\,, \tag{3.5}$$

where the Lorentz boost has been approximated in the low Fermi momentum limit and $(p_{p\|}, \boldsymbol{p}_{p\perp})$ are the components of the final-proton momentum $\boldsymbol{p}_p$ parallel and perpendicular to the momentum $\boldsymbol{p}$ of the incident deuteron, which has energy E_{di}.

4 The triangle diagram

The triangle diagram of fig. 1b requires as input the amplitudes for the sub-reactions $NN \to NN\eta$. The threshold c.m. amplitudes for $I = 1$ and $I = 0$ are, respectively,

$$\mathcal{M}_1(NN \to NN\eta) = \left[\,\mathcal{W}_{1,s}\,\eta_f^\dagger\,\hat{p}\cdot\boldsymbol{\epsilon}_i\,\right]\,\boldsymbol{\chi}_f^\dagger \cdot \boldsymbol{\chi}_i\,, \tag{4.1}$$

$$\mathcal{M}_0(NN \to NN\eta) = \left[\,\mathcal{W}_{0,t}\,\hat{p}\cdot\boldsymbol{\epsilon}_f^\dagger\,\eta_i\,\right]\,\phi_f^\dagger\,\phi_i\,, \tag{4.2}$$

where $\boldsymbol{\chi}$ and ϕ represent the isospin-1 and isospin-0 configurations of the NN states, with $\boldsymbol{\epsilon}$ and η corresponding to the spin-1 and spin-0 combinations.

The spin-averaged total η-production cross-sections are

$$\begin{aligned}\sigma(pp\to pp\eta) &= \frac{1}{2048\pi^2 p_{NN} s_{NN}}\,\frac{m_N}{\left(1+2m_N/m_\eta\right)^{1/2}} \\ &\quad\times Q_{NN\eta}^2\,|\mathcal{W}_{1,s}|^2\,, \\ \sigma(pn\to pn\eta) &= \frac{1}{4096\pi^2 p_{NN} s_{NN}}\,\frac{m_N}{\left(1+2m_N/m_\eta\right)^{1/2}} \\ &\quad\times Q_{NN\eta}^2\left[|\mathcal{W}_{1,s}|^2 + |\mathcal{W}_{0,t}|^2\right]\,,\end{aligned} \tag{4.3}$$

where p_{NN} and s_{NN} are the momentum and square of the total energy in the c.m. system, m_N the nucleon mass, and $Q_{NN\eta}$ the excess energy in the final system [11].

In terms of an initial deuteron momentum $-\boldsymbol{p}$, a final-deuteron momentum $\boldsymbol{p}_d$, and a momentum transfer $\boldsymbol{Q} = \boldsymbol{p}_d + \boldsymbol{p}$, the triangle graph is evaluated in the standard way by putting the *spectator* nucleon on-shell at an average energy $E_N(\frac{1}{2}\boldsymbol{p})$. The spin-averaged matrix element becomes

$$\begin{aligned}&\frac{1}{6}\sum_{\text{spin}} |\,\mathcal{M}(pd \to pd\eta)\,|^2 = \frac{1}{64}\left(\frac{m_d}{E_{di}}\right)^2 \\ &\times\left[|3W_{1,s} + W_{0,t}|^2\,\left[S_S^2(\tfrac{1}{2}Q) + S_Q^2(\tfrac{1}{2}Q) + \tfrac{2}{3}S_A^2(\tfrac{1}{2}Q)\right]\right. \\ &\left.+|3W_{1,s} - W_{0,t}|^2\,\tfrac{4}{3}S_M^2(\tfrac{1}{2}Q)\right]\,.\end{aligned} \tag{4.4}$$

The spherical, quadrupole, magnetic and axial form factors appearing here are defined by

$$\begin{aligned}S_S(Q) &= S_a(Q) + S_b(Q)\,, \\ S_Q(Q) &= 2S_c(Q) - S_d(Q)/\sqrt{2}\,, \\ S_M(Q) &= S_a(Q) - \tfrac{1}{2}S_b(Q) + S_c(Q)/\sqrt{2} + \tfrac{1}{2}S_d(Q)\,, \\ S_A(Q) &= S_a(Q) - \tfrac{1}{2}S_b(Q) - \sqrt{2}S_c(Q) - S_d(Q)\,,\end{aligned} \tag{4.5}$$

where the terms on the right-hand side represent integrals over the reduced deuteron wave functions (u and w):

$$\begin{aligned}S_a(Q) &= \int_0^\infty j_0(Qr)\,\left[u(r)\right]^2\,\mathrm{d}r\,, \\ S_b(Q) &= \int_0^\infty j_0(Qr)\,\left[w(r)\right]^2\,\mathrm{d}r\,, \\ S_c(Q) &= \int_0^\infty j_2(Qr)\,u(r)w(r)\,\mathrm{d}r\,, \\ S_d(Q) &= \int_0^\infty j_2(Qr)\,\left[w(r)\right]^2\,\mathrm{d}r\,.\end{aligned} \tag{4.6}$$

Experimental data on η production in pp [12] and pn [13] collisions above the *fsi* regions show that $|W_{1,s}|^2 \approx 0.76\times10^9$ μb and $|W_{0,t}|^2 \approx 9.2\times10^9$ μb, though the relative phase of these two amplitudes is not determined. In a meson-exchange approach, it is suggested that ρ-exchange is the largest term [11]. If further we take the two amplitudes to be in phase then we find that

$$|3\mathcal{W}_{1,s}+\mathcal{W}_{0,t}|^2 = 3.2\times10^{10}\,\mu\mathrm{b}\,,$$
$$|3\mathcal{W}_{1,s}-\mathcal{W}_{0,t}|^2 = 1.6\times10^{8}\,\mu\mathrm{b}\,. \qquad (4.7)$$

5 The two-step model

The contribution of the two-step model with an intermediate pion can be estimated using the same techniques as for the more complicated $p\,d\to{}^3\mathrm{He}\,\eta$ reaction, where there are two integration loops over the unobserved Fermi momenta [4]. In terms of the internal momenta marked in fig. 1c, the $p\,d\to p\,d\,\eta$ matrix element becomes

$$\mathcal{M} = \frac{\sqrt{2m_d}}{(2\pi)^{3/2}}\int \mathrm{d}^3q' \sum_{\mathrm{int}} \mathcal{M}(\pi^+n\to\eta\,p) \times\frac{-i}{2E_\pi(\sqrt{s}-E_{\mathrm{int}}+i\varepsilon)}\mathcal{M}(pp\to\pi^+d)\,\tilde\Psi(\boldsymbol{q}')\,, \quad (5.1)$$

where the sum runs over the internal spin indices.

The pion propagator between the matrix elements for the production and conversion of the pion in eq. (5.1) has been approximated by its positive energy pole. The difference between the external and internal energies, $\Delta E = \sqrt{s}-E_{\mathrm{int}}$, depends upon the Fermi momentum $\boldsymbol{q}$ and, following ref. [4], we retain only linear terms in this integration variable:

$$\Delta E = \sqrt{s}-E_d(\boldsymbol{p}_d)-E_n(-\tfrac12\boldsymbol{p}+\boldsymbol{q})-E_\pi(\tfrac12\boldsymbol{p}-\boldsymbol{q}-\boldsymbol{p}_d) \approx \Delta E_0+\boldsymbol{V}\cdot\boldsymbol{q}\,, \quad (5.2)$$

where the mean energy defect

$$\Delta E_0 = \sqrt{s}-E_d(\boldsymbol{p}_d)-E_n(-\tfrac12\boldsymbol{p})-E_\pi(\tfrac12\boldsymbol{p}-\boldsymbol{p}_d) \quad (5.3)$$

and the relativistic relative velocity between the pion and neutron

$$\boldsymbol{V} = \boldsymbol{v}_\pi-\boldsymbol{v}_n = \left(\frac{E_n+E_\pi}{2E_nE_\pi}\right)\boldsymbol{p}-\frac{1}{E_\pi}\boldsymbol{p}_d \quad (5.4)$$

do not depend on the proton or η momenta in the final state.

Both the argument of the deuteron momentum space wave function $\tilde\Psi(\boldsymbol{q}')$ and the integration variable are the Fermi momentum $\boldsymbol{q}'$, Lorentz contracted in the beam direction; $\boldsymbol{q}'_\perp=\boldsymbol{q}_\perp$, $\boldsymbol{q}'_\parallel=\boldsymbol{q}_\parallel/\gamma$, with $\gamma=E_d(p)/m_d\approx E_n(-\frac12 p)/m_n$.

The linearisation is valid only if relatively small Fermi momenta are required to allow the two steps to proceed almost on-shell, which means that the energy defect should be small. At the η-production threshold $\Delta E_0\approx-15$ MeV, which illustrates the *kinematic miracle* first noted for the $p\,d\to{}^3\mathrm{He}\,\eta$ reaction [3]. We then neglect the dependence of the individual $pp\to\pi^+d$ and $\pi^+n\to\eta p$ amplitudes upon the Fermi momentum so that the only place where $\boldsymbol{q}$ occurs is in the denominator of the propagator. By defining a Lorentz transformed velocity with components

$$\boldsymbol{V}'_\perp=\boldsymbol{V}_\perp \;\text{ and }\; \boldsymbol{V}'_\parallel=\gamma\boldsymbol{V}_\parallel \quad (5.5)$$

the whole integrand can be written in terms of $\boldsymbol{q}'$.

After decomposing the deuteron wave function into its $\ell=0,\,2$ components, we are left with integrals of the form

$$i\int \mathrm{d}^3q'\frac{\tilde\varphi_\ell(q')T_\ell(\hat{\boldsymbol{q}}')}{\Delta E_0+\boldsymbol{V}'\cdot\boldsymbol{q}'+i\varepsilon} = \int_0^\infty \mathrm{d}t\,e^{i(\Delta E_0+i\varepsilon)t} \times\int_0^\infty q'^2\,\mathrm{d}q'\varphi_\ell(q')\int\mathrm{d}\Omega_{q'}\,e^{it\boldsymbol{V}'\cdot\boldsymbol{q}'}\,T_\ell(\hat{\boldsymbol{q}}') = S_\ell(\Delta E_0,|\boldsymbol{V}'|)\,T_\ell(\hat{\boldsymbol{V}}')\,, \quad (5.6)$$

where the S- and D-state form factors involve integrals over the *configuration-space* deuteron wave functions

$$S_\ell(\Delta E_0,|\boldsymbol{V}'|) = \frac{(2\pi)^{3/2}}{|\boldsymbol{V}'|}\int_0^\infty \mathrm{d}t\,e^{i\omega t}\,\varphi_\ell(t) \quad (5.7)$$

with $\omega=\Delta E_0/|\boldsymbol{V}'|$.

The s-wave nature of the $S_{11}(1535)$-resonance that dominates low-energy η production in $\pi^+n\to\eta\,p$, leads to largely isotropic production at low energies. We can then take the matrix element to be proportional to the corresponding spin–non-flip amplitude

$$\mathcal{M}(\pi^+n\to\eta\,p) = \frac{4\pi\sqrt{s_{\eta p}}}{m}\,f(\pi^+n\to\eta\,p)\,. \quad (5.8)$$

For simplicity, of the six invariant $pp\to\pi^+d$ amplitudes we shall keep only the largest in our energy region, for which

$$\mathcal{M}(pp\to\pi^+d) = -\sqrt{2}\,\mathcal{A}\,(\boldsymbol{\epsilon}_d^\dagger\cdot\hat{\boldsymbol{p}}_\pi)\,\phi_{pp}\,, \quad (5.9)$$

where ϕ_{pp} and $\boldsymbol{\epsilon}_d$ represent the spin-zero and spin-one initial and final NN states. This is then related to the c.m. cross-section through

$$|\mathcal{A}\,|^2 = 8(2\pi)^2\left\{\frac{s_{pp}}{m^2}\frac{p_p}{p_\pi}\frac{\mathrm{d}\sigma}{\mathrm{d}\Omega}(pp\to\pi^+d)\right\}_{\mathrm{c.m.}}. \quad (5.10)$$

In addition to the π^+ diagram of fig. 1c, there is also the possibility of π^0 propagation between the two steps. This can be taken into account by simply multiplying the matrix element $\mathcal{M}$ of eq. (5.1) by an isospin factor of 3/2. Using eq. (2.2), we then arrive at an expression for the distribution of the $p\,d\to p\,d\,\eta$ cross-section in terms of the final-deuteron angles and ηp invariant mass:

$$\frac{\mathrm{d}^2\sigma}{\mathrm{d}\Omega_d\,\mathrm{d}m_{\eta p}} = \frac{9}{4(2\pi)^4}\,\frac{s_{\eta p}\,m_d\,p_d\,p_\eta^*}{s\,p\,E_\pi^2}\left(|S_S|^2+|S_D|^2\right) \times\left\{\frac{s_{pp}}{m^2}\frac{p_p}{p_\pi}\frac{\mathrm{d}\sigma}{\mathrm{d}\Omega}(pp\to\pi^+d)\right\}_{\mathrm{c.m.}} \times\left\{\frac{p_\pi}{p_\eta}\sigma_{\mathrm{tot}}(\pi^+n\to\eta\,p)\right\}_{\mathrm{c.m.}}, \quad (5.11)$$

where we have taken advantage of the isotropy of the $\pi^+ n \to \eta\, p$ differential cross-section to integrate over the η angles and to write the result in terms of the total cross-section. This option is not open for the other differential distributions, where extra non-trivial integrations have to be performed.

An effective range description of the low-energy $\pi^+ n \to \eta\, p$ total cross-section is

$$\frac{p_\pi^*}{p_\eta^*}\sigma_{\rm tot}(\pi^+ n \to \eta\, p) \approx \frac{2.76|a|^2}{\left|1 - iap_\eta^* + \frac{1}{2}r_0 a p_\eta^{*2}\right|^2}\,. \qquad (5.12)$$

The data base has not improved significantly since we took the values $a = (0.476 + 0.279i)$ fm and $r_0 = (-3.16 - 0.13i)$ fm [4].

The $pp \to \pi^+ d$ cross-sections are obtainable from the SAID analysis [14] but, because the intermediate pion in fig. 1a is non-physical, some prescription is needed to extrapolate from the experimental data. We have assumed in the applications that the amplitudes are unchanged when the c.m. production angle is kept fixed.

6 Comparison with experiment

The predictions of the three driving terms of fig. 1 are compared in fig. 2 with the existing experimental data [6,8]. It is immediately apparent that the impulse approximation of the triangle graph in fig. 1b lies well over an order of magnitude below the experimental data. The ambiguity in the relative phase of the amplitudes $\mathcal{W}_{1,s}$ and $\mathcal{W}_{0,t}$ is therefore largely irrelevant and the impulse approximation term will in general be dropped from further discussion.

In the near-threshold region of low Q, the two-step contribution dominates that of the pick-up by an order of magnitude. The kinematics here are somewhat similar to those of low-energy $p\,d \to {}^3\mathrm{He}\,\eta$ reaction where the pick-up term with a proton-deuteron final-state interaction similarly underpredicts the experimental data [15,2]. However, the two-step term levels off at $Q \approx 80$ MeV and eventually decreases at higher energies due to a combination of factors. The region where the intermediate pion is close to being physical becomes a smaller fraction of the allowed phase space but also the $pp \to d\pi^+$ cross-section falls steeply above the Δ region. Since the pick-up term must approach that for quasi-free $pn \to d\eta$ above the NN threshold, the two contributions must cross before then. In our estimates, this occurs at $Q \approx 95$ MeV.

The incoherent sum of the three contributions is also shown in fig. 2. Though the shape is very similar to that of the experimental data, these lie about a factor of 1.7 above the curve at high energies and a little bit more nearer threshold. This parallels a similar underprediction of the $p\,d \to {}^3\mathrm{He}\,\eta$ reaction in a two-step model that includes the effects of the $\eta\,{}^3$He *fsi* [4]. The fractions of phase space where the pd or ηd final-state interactions might enhance the $p\,d\,\eta$ channel are relatively small at the higher energies.

More information can be derived from the differential distributions that were measured at $T_p = 1032$ MeV

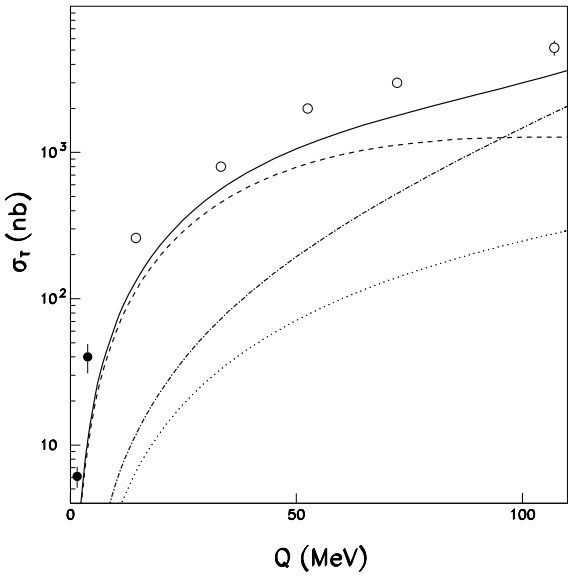

Fig. 2. Total cross-section for the reaction $p\,d \to p\,d\,\eta$. The experimental data are taken from Saclay (solid circles) [6] and CELSIUS (open circles) [8]. The dotted curve represents the predictions of the triangle diagram (impulse approximation), the chain curve the pick-up contribution, and the dashed curve that of the two-step model. The incoherent sum of these three terms is shown by the solid curve.

($Q = 72.3$ MeV) [8]. The only significant enhancement in the three invariant-mass distributions of fig. 3 is that near the ηd threshold, which is consistent with the large scattering length suggested by the low-energy $pn \to d\eta$ total cross-section data [10]. In contrast, despite the existence of the nearby ^{3}He bound-state pole, there is no sign of any *pd fsi*. The two-step model leads to only minor distortions of the invariant-mass phase spaces, pushing $m_{p\eta}$ to slightly larger values, whereas the pick-up contribution preferentially populates low $m_{d\eta}$ masses which is reflected kinematically as a slight increase at higher values of m_{pd}.

Apart from the overall strength being too low by a factor of two, the sums of the two contributions give plausible descriptions of the invariant-mass distributions but the same cannot be said for the angular distributions shown in fig. 4. In the pick-up contribution of fig. 1a, the final proton is a spectator and the transverse momentum is governed by the Fermi momentum components in the deuteron. This automatically gives a sharp peak for a c.m. proton angle close to the backward direction and this has a slightly weaker kinematic reflection around the forward deuteron direction. Given that the estimate within the pick-up model has relatively few uncertainties, the discrepancy with the experimental data of ref. [8] is particularly significant.

There are far more uncertainties in the evaluation of the two-step model since the intermediate pion is generally off its mass shell and this affects the kinematics of the

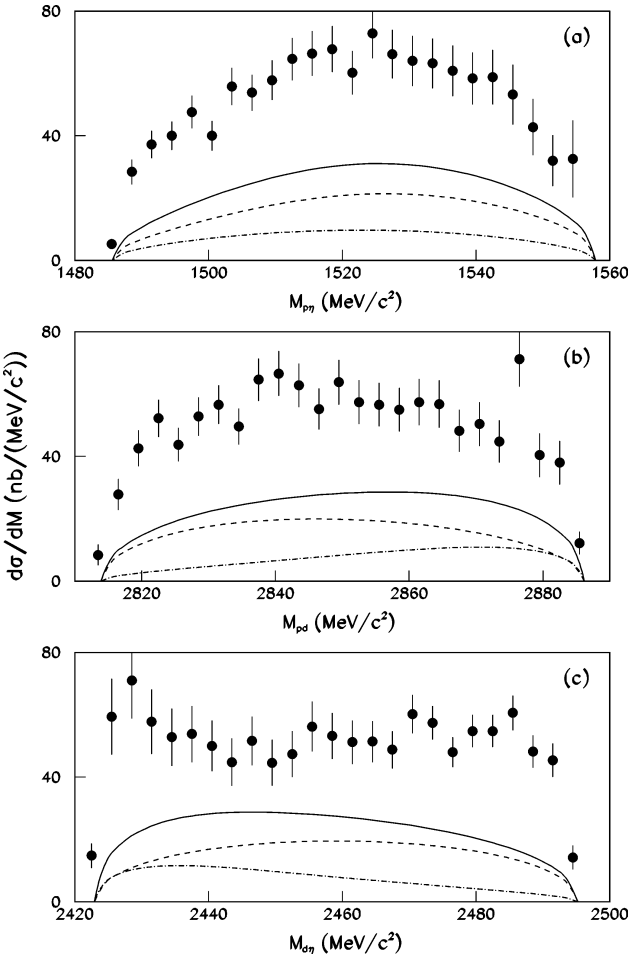

Fig. 3. Distributions in the invariant masses of the $p\,d \to p\,d\,\eta$ reaction at $Q = 72.3$ MeV. The panels (a), (b), and (c) refer, respectively, to the $p\eta$, pd, and $d\eta$ cases. The experimental data from ref. [8] are compared to the predictions of the pick-up term (chain curve), the two-step model (dashed curve), and their incoherent sum (solid curve).

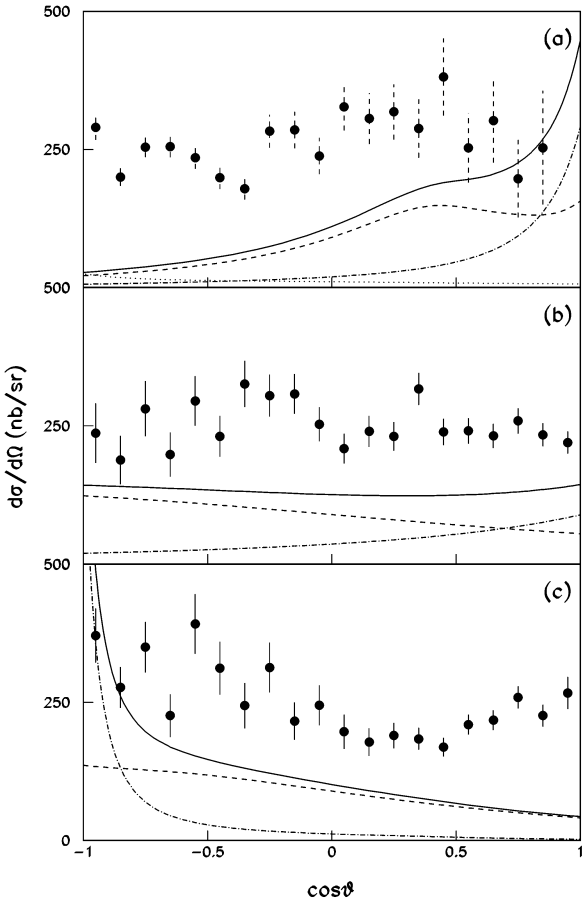

Fig. 4. Centre-of-mass angular distributions with respect to the incident proton direction of the $p\,d \to p\,d\,\eta$ reaction at $Q = 72.3$ MeV. The panels (a), (b), and (c) refer, respectively, to outgoing d, η, and p. The experimental data from ref. [8] are compared to the predictions of the pick-up term (chain curve), the two-step model (dashed curve), and their incoherent sum (solid curve). The impulse approximation contribution, shown by the dotted curve for the deuteron case, lies well below the experimental data even at large angles.

$pp \to d\pi^+$ reaction. However, the deuteron angular distribution of fig. 4a does suggest that the models need to be supplemented at large angles and this might be the reason for the underestimation of the total cross-section. The results of the impulse approximation shown in this panel would have to be increased by an order of magnitude to fill the gap.

7 Conclusions

We have estimated the contributions of three different models to the total and partial cross-sections of the $p\,d \to p\,d\,\eta$ reaction below the η-production threshold in nucleon-nucleon collisions. The impulse approximation turns out to be generally negligible compared to the other two terms of which the two-step model is shown to be dominant in the near-threshold region. However, although some of our kinematic approximations may start to break down before one reaches the free pn threshold ($Q \approx 192$ MeV), the estimates suggest that the two-step mechanism would provide only a very small correction to the pick-up interpretation of the CELSIUS quasi-free $pn \to d\eta$ data [10].

We have neglected the final-state interactions which should distort the lower edges of the invariant-mass distributions shown in fig. 3 while having a smaller effect on the total cross-section away from the threshold region. In fact the only *fsi* clearly seen in the experimental data is that associated with the ηd channel [8]. Now the total cross-section at the higher energies is underestimated by almost a factor of two, which is a very similar factor to that found for the near-threshold two-body $p\,d \to {}^3\mathrm{He}\,\eta$ reaction interpreted in the same two-step approach, after the inclusion of the necessary *fsi* effects [4]. It is, however, intriguing to note that, although there is no sign of

the strong *pd fsi* in the experimental data of fig. 3b, the normalisation of the total $p\,d \to p\,d\,\eta$ total cross-section is predicted successfully from the $p\,d \to {}^3\mathrm{He}\,\eta$ data using the final-state extrapolation theorem [16] without implementing a full dynamical model.

Apart from the *fsi* regions, it is hard to draw firm conclusions on the models from the invariant-mass distributions of fig. 3. There is far more information to be gleaned from the angular distributions of fig. 4. The models underpredict the data in the backward deuteron hemisphere and, more critically, there is no sign in the data for the sharp peaks for forward-going deuterons and backward-going protons being produced in the pick-up process. Although these might be softened somewhat by multiple scatterings or *fsi*, it should also be noted that if either the deuteron *or* the proton is lost down the beam pipe then the event is not registered [8].

If indeed the two-step model is the dominant mechanism well below the nucleon-nucleon threshold, it would have consequences for the $p\,d \to ppn\eta$ four-body final state, where one could expect to see a strong *pn fsi*. Data on this reaction were taken at CELSIUS simultaneously with those on the other channels, but their detailed analysis is not yet complete [17]. Data also exist from COSY on the analogous sub-threshold $p\,d \to K^+\Lambda\,d$ reaction [18] and it would seem likely that the corresponding two-step model should play an important role there as well.

We are much indebted to our colleagues in Uppsala, especially J. Złomańczuk, for discussions regarding the η-production programme at CELSIUS. One of the authors (C.W.) is grateful for financial support and hospitality from both the Department of Radiation Sciences and the The Svedberg Laboratory of the University of Uppsala. Comments by Y. Uzikov regarding the impulse approximation term proved helpful.

References

1. J. Berger *et al.*, Phys. Rev. Lett. **61**, 919 (1998).
2. J.-F. Germond, C. Wilkin, J. Phys. G **15**, 437 (1989).
3. K. Kilian, H. Nann, AIP Conf. Proc. **221**, 185, (1990).
4. G. Fäldt, C. Wilkin, Nucl. Phys. A **587**, 769 (1995).
5. B. Mayer *et al.*, Phys. Rev. C **53**, 2068, (1996).
6. F. Hibou *et al.*, Eur. Phys. J. A **7**, 537, (2000).
7. U. Tengblad, TSL/ISV Report No. 96-0163 (1996), unpublished.
8. R. Bilger *et al.*, Phys. Rev. C **69**, 014003, (2004).
9. R. Bilger *et al.*, Phys. Rev. C **65**, 044608 (2002).
10. H. Calén *et al.*, Phys. Rev. Lett. **79**, 2642, (1997); H. Calén *et al.*, Phys. Rev. Lett. **80**, 2069, (1998).
11. G. Fäldt, C. Wilkin, Phys. Scr. **64**, 427, (2001).
12. H. Calén *et al.*, Phys. Lett. B **366**, 39, (1996).
13. H. Calén *et al.*, Phys. Rev. C **58**, 2667, (1998).
14. R. Arndt *et al.*, Phys. Rev. C **48**, 1926, (1993); `http://gwdac.phys.gwu.edu/`.
15. J.-M. Laget, J.-F. Lecolley, Phys. Rev. Lett. **61**, 2069, (1988).
16. G. Fäldt, C. Wilkin, Phys. Lett. B **382**, 209, (1996).
17. J. Złomańczuk, private communication.
18. Y. Valdau, private communication.